

Size modulated transition in the fluid-structure interaction losses in nano mechanical beam resonators

S. D. Vishwakarma,[1] A. K. Pandey,[2, a)] J. M. Parpia,[3] S. S. Verbridge,[4] H. G. Craighead,[3] and R. Pratap[1, b)]

[1)] *Center for Nano Science and Engineering, Indian Institute of Science, Bengaluru 560012, India*

[2)] *Department of Mechanical Engineering, Indian Institute of Technology, Hyderabad 502285, India*

[3)] *Center for Materials Research, Cornell University, Ithaca, New York 14853, USA*

[4)] *Biomedical Engineering and Mechanics, Virginia Tech, Blacksburg, VA 24061, USA*

(Dated: 7 April 2016)

An understanding of the dominant dissipative mechanisms is crucial for the design of a high-Q doubly clamped nanobeam resonator to be operated in air. We focus on quantifying analytically the viscous losses—the squeeze film damping and drag force damping—that limit the net quality factor of a beam resonator, vibrating in its flexural fundamental mode with the surrounding fluid as air at atmospheric pressure. Specifically, drag force damping dominates at smaller beam widths and squeeze film losses dominate at **larger** beam widths, with no significant contribution from structural losses and acoustic radiation losses. The combined viscous losses agree well with the experimentally measured Q of the resonator over a large range of beam widths, within the limits of thin beam theory. We propose an empirical relation between the maximum quality factor and the ratio of maximum beam width to the squeeze film air gap thickness.

Keywords: MEMS, NEMS, Drag force, Squeeze film damping

[a)] Electronic mail: ashok@iith.ac.in

[b)] Electronic mail: pratap@mecheng.iisc.ernet.in

I. INTRODUCTION

The sensitivity of flexural nanobeam resonators to changes in various physical quantities such as temperature, pressure, and mass (m),[1–3] is most often expressed in terms of the change in resonant frequency (f). The sensitivity to the physical quantities under assay ($\delta m/m$) varies as ($\delta f/f$) or inversely as the quality factor (Q). While the Q can be improved by operating the devices in vacuum[4,5], sensing is often most practically carried out when the device operates in air under ambient conditions. These devices are influenced by fluid-structure interaction losses (squeeze film damping and drag force damping) that limit the Q at ambient pressure. Studies reveal that one or the other of these damping mechanisms dominates. Reliably achieving higher Q requires a better understanding of the damping mechanisms and the role of geometry on the magnitude of the damping.

The quality factor or Q-factor is a physical parameter that quantifies the ratio of energy stored (or maximum kinetic energy of the resonator), to the energy dissipated, per cycle of oscillation of the resonator. The net dissipation is obtained by **summing** the dominant sources of dissipation, namely, squeeze film damping (sq), drag force damping (dr), acoustic radiation damping (ac), thermoelastic damping (ted), and clamping losses (cl) denoted by their corresponding subscripts, and the net Q in terms of corresponding Q's is given by[6]

$$Q_{\text{net}}^{-1} = Q_{\text{sq}}^{-1} + Q_{\text{dr}}^{-1} + Q_{\text{ac}}^{-1} + Q_{\text{ted}}^{-1} + Q_{\text{cl}}^{-1}. \tag{1}$$

The quality factor associated with the structural losses such as thermoelastic losses[7] and clamping losses[8] are found to be of the order of $O(10^6)$. Hence there is a marginal contribution of structural losses to the measured quality factor corresponding to various beam **widths**. For doubly clamped beams, the quality factor associated with the acoustic losses[9] is of the order of $O(10^3)$ and also found to contribute marginally to the experimentally measured quality factors, rendering the viscous losses in the form of drag and squeeze film to **be dominant**.

Ikehala *et al.*[10] investigated the variation in the Q of a microscale cantilever beam with width by modeling the drag force on the vibrating beam with an equivalent vibrating sphere model. They computed the drag force from an effective spherical radius and compared **the computed results** with measured values. However, the dependency on width was found to be insignificant. Xia and Li[11] studied the effects of air drag on a cantilever operating in

different modes under ambient conditions. They used the dish-string model for the air drag and compared the calculated values with numerical and experimental results. Verbridge *et al.*[12] found that the measured quality factor of doubly clamped beam resonators, operated in air in their fundamental out-of-plane mode vibration, scale as the ratio of volume to surface area of the resonator. **For small widths,** as the beam width is increased, the Q also increases. Depending on the size of the air gap between the device and the stationary substrate (the air in the gap constitutes the squeeze film), a maximum in Q is attained at a particular width, and a further increase in a device width results in a reduced Q due to the **increase in** squeeze film damping. **For larger air gaps, the width corresponding to the highest Q also increases. However, despite the measurement of the variation of quality factor with beam width, the identification of the dominant damping mechanism as a function of the beam width was uncertain.** To understand the variation in quality factor of a cantilever beam near a fixed plate, **the theoretical damping force needs to be quantified in terms of the beam length**, width, and the air-gap thickness. Bullard *et al.*[13] and Sadar *et al.*[14] have presented dynamic similarity laws and generalized scaling laws, respectively, to capture drag forces due to the vibration of cantilever beam with and without a nearby fixed plate. While Ramanathan *et al.*[15] have presented a 1D model under continuum and free molecular regime, Lissandrello *et al.*[16] have presented a model which requires the computation of the fitting parameters from experimental or numerical studies. To model the damping effect of an AFM cantilever beam near the rigid surface under different flow regimes and air-gap thickness, Drezet *et al.*[17] and Honig *et al.*[18], Bowles and Ducker[19] have introduced a slip length to be used on both the surfaces. They found that the magnitude of slip also depended on the nature of the fluid-solid interface. While Honig *et al.*[18] and Bowles and Ducker[19] have presented their studies based on a modified 1D model of drag forces incorporating slip lengths and air-gap thickness, Drezet *et al.*[17] have presented a 2D model based on the lubrication theory by introducing a slip length on both the surfaces of a cantilever under uniform or rigid motion. The success of these models depends on finding the correct slip lengths and their scaling. Although these cited studies have presented different models to compute drag forces near and away from a fixed plate with rarefaction effects, most of them are based on 1D model except the one proposed by Drezet *et al.*[17]. Moreover, none of them have discussed the influence of width on the combined effect of drag forces and squeeze film on the quality factor **necessary to**

allow the computation of $Q_{\max}$ corresponding to a particular beam width. Consequently, they cannot be used in their present form to capture both the effects together.

In the present study, we identify and quantify the dominant dissipative mechanisms that depend on the beam width of a nanomechanical fixed-fixed beam. Our study not only solves the long **standing problem concerning the uncertainty of when drag effects dominate over squeeze-film damping (and vice-versa)** but also provides design guidelines to achieve optimum quality factor associated with the fundamental mode of such resonators operated in air. We find that the viscous losses **(squeeze film damping and drag force losses)** are the dominant dissipative mechanisms that contribute in different proportions with varying beam widths. To identify the correct models, we compare different drag force and squeeze film models individually with experimental results. Later, we use the optimized drag and squeeze film models to capture the combined effects at various beam widths and air-gap thicknesses that agrees well with the measurements of Verbridge *et al.*[12]. Using the optimized models, we analyze the variation of maximum quality factor with different width to air-gap ratio and length to width ratio respectively. Finally, we propose **an** empirical model to capture such variations.

II. VISCOUS LOSSES IN THE DOUBLY CLAMPED BEAM

To study the influence of beam width and air-gap thickness of a fixed-fixed beam on fluid damping, we take the dimensions and properties of the beam from Verbridge *et al.*[12] as shown in Fig. 1. The beam is fabricated with silicon nitride material with Young's modulus, $E = 200$ GPa, Poisson ratio, $\nu = 0.23$ and mass density, $\rho_s = 2800$ kg/m^3. The nominal and effective beam length including the undercut dimension of 1.5 μm are taken as $a = 11$ μm and $a_c = 12.5$ μm, respectively. To compute fluid damping, we take the effective length of the beam. Each beam has a thickness of $d_0 = 140$ nm and varying width, b, from 55 nm to 1910 nm. The beams are separated from the bottom substrate by the air-gap thicknesses of $h_0 = 250$ nm, 460 nm, 660 nm, and 750 nm, respectively. The measured values of in-vacuo fundamental frequencies are taken as 13-14 MHz. However, the theoretical frequency value subjected to residual stress of σ_r can be obtained based on approximate modeshape $\phi(x) = (1 - cos(2\pi x/a))/2$ from the formula

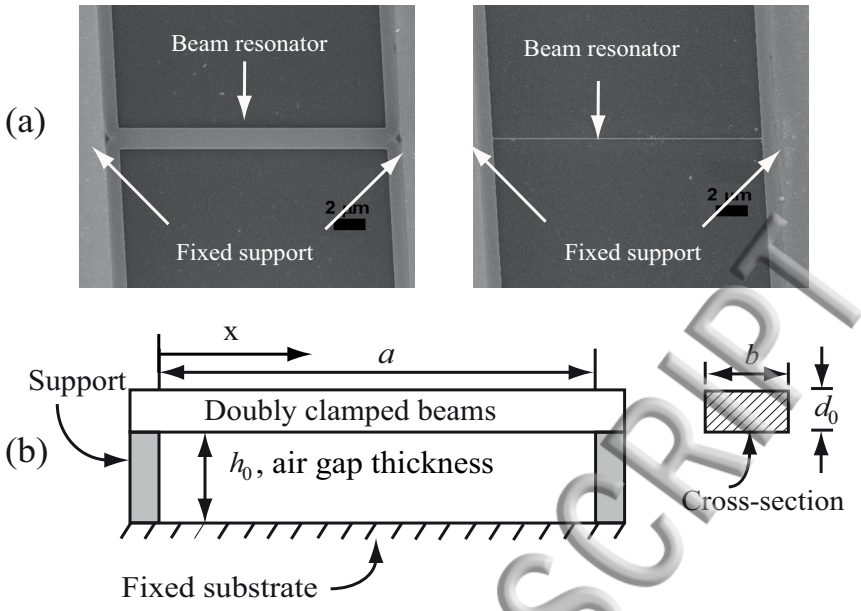

FIG. 1. (a) SEM images showing the top view of two beams with different width (1.5 μm and 50 nm wide, respectively); (b) Schematic of a doubly clamped beam (front view), with length, $a = 11$ μm, varying width, b, thickness, $d_0 = 140$ nm, suspended above the thin air film of thickness h_0.

based on Rayleigh method as[9,20]

$$\omega_a^2 = \frac{(2\pi)^2}{3}\left(\frac{E(bd_0^3/12)}{\rho_a(bd_0)}\right)\frac{1}{a^4} + \frac{(2\pi)^2}{3}\left(\frac{\sigma_r}{\rho_s}\right)\frac{1}{a^2}. \quad (2)$$

For the given dimensions and material properties, we find the frequency of 13 MHz corresponding to a residual stress of 140 MPa. Since the beam vibrates in air, we take the air viscosity, $\mu = 18.3\times10^{-6}$ Ns/m^2, density, $\rho_f = 1.2$ kg/m^3, pressure, $P_a = 1.013\times10^5$ N/m^2 and temperature 300 K. At ambient temperature and pressure, the speed of sound is found as $c_s = 343.2$ m/s, the mean molecular speed $u_{\text{th}} = 468.23$ m/s, the mean free path of air as $\lambda = 67$nm, and the boundary layer thickness $\delta = \sqrt{2\mu/\rho_f\omega} = 611$ nm. For the first mode of vibration of a fixed-fixed beam, the effective mass $m_e = 0.375\rho_s a_c b d_0$, and the effective stiffness $k_e = \omega_a^2 m_e$.

A. Flow Characterization

To quantify the viscous losses and predict the size effects on the measured quality factor of doubly clamped beams operated in their fundamental mode at identical frequencies but with varying beam widths, we compute various non-dimensional numbers such as the Knudsen

number, Reynolds number, aspect ratio, etc. For a given beam length a and varying air-gap thickness h_0 and beam width b, the Knudsen numbers and the Reynolds numbers based on the different characteristics length scale can be computed as[6,15,21,22]

- $\mathrm{Kn_h} = \frac{\lambda}{h_0}$: It is used to define the degree of rarefaction in squeeze film damping. For the airgap thickness $h_0 = 250$nm, 460 nm, 660nm, and 750nm, the Knudsen number is found to be 0.27 (Transition), 0.14 (Transition), 0.10 (Slip) and 0.09 (Slip). Therefore, the effect of rarefaction needs to be considered in squeeze film force computation. It can be captured by computing the effective viscosity[23,24].

- $\mathrm{Kn_b} = \frac{\lambda}{b}$: It is used to define degree of rarefaction when the beam is far away from the fixed plate. For beam width of $b = 50$ nm to $2\mu m$, $\mathrm{Kn_b}$ varies from 1.34 (transition flow) to 0.03 (slip flow). The effect of rarefaction needs to be considered in drag force computation.

- $\mathrm{Kn}_\delta = \frac{\lambda}{\delta} = \sqrt{\omega\tau}$: For $\delta = 611$ nm and, we get $\mathrm{Kn}_\delta = 0.109 < 1$. Since, the Weissenberg number Wi=$\omega\tau < 1$, the flow can be assumed to be quasisteady flow.

- $\mathrm{Re_h} = \frac{\rho_f \omega h_0^2}{\mu} = \frac{2h_0^2}{\delta^2}$: For the airgap thickness h =250 nm, 460 nm, 660 nm, and 750 nm, $\mathrm{Re_h}$ varies from 0.33 1.13, 2.3, 3 for a frequency of 13 MHz. The values show that the local inertial effect is important for large air-gap. **Alternatively, the ratio $\frac{h_0}{\delta}$ can also be used to characterize the flow as being in the static regime ($h_0 >> \delta$) or in the dynamic regime ($h_0 \approx \delta$) in the case of the squeeze film damping.**

- $\mathrm{Re_b} = \frac{(\rho_f \omega b^2)}{\mu} = \frac{2b^2}{\delta^2}$: For a beam width of $b = 50$ nm, 420 nm 590nm, 1000 nm, 2000 nm, $\mathrm{Re_b}$ varies from 0.014, 1.01, 2.01, 5.76, to 23. For beam widths greater than 400 nm, the inertial effect in drag force become significant. **As in the previous case, the ratio $\frac{b}{\delta}$ signifies the static regime ($b >> \delta$) and the dynamic regime for ($b \approx \delta$) in the case of drag forces.**

- $\mathrm{Re_c} = \frac{(\rho_f \omega \delta_z b)}{\mu}$: For small oscillations, $\delta z \approx 1$nm, $\mathrm{Re_c}$ is negligibly small. Consequently, the convective inertia term can be neglected.

The computation of these different Knudsen and the Reynolds numbers show that rarefaction and inertial effects are important in computing damping due

This manuscript was accepted by J. Appl. Phys. Click here to see the version of record.

ng squeeze film and drag forces. Since, the ratio, h_0/b, is greater than 0.1, the effect associated with 3D flow should also be considered in the formulations of drag force and damping. Now, we describe different models of drag and squeeze film damping under different operating conditions.

B. Different Analytical Models

There exist several different models to compute drag forces with or without nearby fixed plate and squeeze film damping. We outline some important models and their assumptions below.

1. Drag Force Models

In this section, we describe three important models to compute drag forces under different operating conditions for a beam of width b, thickness d_0, air-gap h_0, operating frequency ω, etc.

- $Q_{\rm d1} = \frac{\rho_s b d_0 \omega}{\gamma_{d1}}$, where, γ_{d1} is the drag force coefficient per unit length. The generalized expression of Stokes drag force coefficient (γ_{d1} per unit length) using **the so-called "sphere"** model[21,25,26] can be reduced to $\gamma_{d1} = 8\mu K_s$ for a thin disk. Therefore, the drag force based quality factor for the slender beam can be written as $Q_{\rm dr} = \frac{\rho_s b d_0 \omega}{8\mu K_s}$. K_s is the scaling factor, introduced to capture all of the terms for the shape correction, rarefaction effect, inertial effect, etc. The factor K_s is independent of air-gap thickness h_0.

- $Q_{\rm d2} = \frac{m_e \omega}{C_2 6\pi \mu_e R_e}$, where $\gamma_{d2} = C_2 6\pi\mu_e R_e$ is the Stokes drag force coefficient, m_e is the effective mass of the beam, $\mu_e = \rho_{fa} u_{\rm th} \lambda$ is the effective viscosity when $\lambda < h$, $u_{\rm th} = \sqrt{8RT/\pi M a}$ $R_a = 27.058$, and $M_a = 28.97$ g/mole. The variation of pressure and temperature can be incorporated in the density as $\rho_{f0} = \sqrt{P/R_a T}$. However, the rarefaction effect can be captured through the mean-free path $\lambda = \mu_f \sqrt{\pi R_a T/2M_a}$ which is inversely proportional to pressure. The effective radius is obtained from $R_e = C_R\sqrt{\frac{a_c b}{\pi}}$, where C_R is the correction in effective radius. This model is independent of air-gap thickness and is valid under low operating frequency such that $R_e << \delta$, where, $\delta = \sqrt{2\mu_e/\rho_{f0}\omega}$[21,25].

This manuscript was accepted by J. Appl. Phys. Click here to see the version of record.

- $Q_{\mathrm{d3}} = \frac{m_e\omega}{C_3 6\pi\mu_e R_e(1+R_e/\delta)}$, where $\gamma_{d3} = C_2 6\pi\mu_e R_e(1+R_e/\delta)$ is the drag force coefficient, $\delta = \sqrt{2\mu_e/\rho_{f0}\omega}$ is the boundary layer thickness and other parameters are same as the previous model Q_{d2}. Like the previous model, this model is also independent of air-gap thickness. However, it is valid for a high operating frequency, i.e., $R_e > \delta_e$. This model can be useful when the characteristic length scale, i.e., beam width, is of same order as the boundary layer thickness[16].

- $Q_{\mathrm{d4}} = \frac{m_e\omega}{\gamma_{d4}}$, where, $\gamma_{d4} = C_4 6\pi\mu_e R_e^2/(h_0 f_f)$, where $f_f = \left[1 + \eta_1 \frac{\lambda}{h_0}\left(1 + \eta_2 \frac{R_e}{\delta_e}\right)\right]$, η_1 and η_2 are the constants based on the strength of $\mathrm{Kn}_h = \lambda/h$ and $\mathrm{Re}_\delta = R_e/\delta_e$, respectively. Unlike the previous models, this model is dependent on air-gap thickness[16].

On comparing different models, we found that Q_{d1}, Q_{d2}, and Q_{d3} are independent of air-gap thickness, and Q_{d4} is dependent on the air-gap thickness. While the inertial effect is captured directly by Q_{d3} and Q_{d4}, the other models capture the effect through fitting parameters.

2. *Squeeze-film Damping Models*

In this section, we discuss two important models to compute squeeze film damping.

- $Q_{\mathrm{s1}} = C_{s1}\frac{m_e\omega}{\gamma_{s1}}$, where, $\gamma_{s1} = \gamma_{\mathrm{pr}} + \gamma_{\mathrm{dp}}$ is the damping coefficient from forces due to pressure and stress at the wall, γ_{pr} and γ_{dp} are given by

$$\gamma_{\mathrm{pr}} = \frac{8A_\gamma a^3 b}{\pi^4}\sum_{n=\mathrm{odd}}\frac{1}{n^4}\left[1 - \frac{2a}{\pi n b}\frac{e^{\pi n b/(2a)} - e^{-\pi n b/(2a)}}{e^{\pi n b/a} - e^{-\pi n b/a}}\right] \tag{3}$$

$$\gamma_{\mathrm{dp}} = -A_\gamma ab\left[h_0^2 - \frac{2b_1 + h_0}{b_0 + b_1 + h_0}(h_0^2 + b_0 h_0)\right], \tag{4}$$

where,

$$A_\gamma = \frac{2\mu}{\rho_f\left[\left(-\frac{1}{3} + \frac{1}{2}\frac{2b_1+h_0}{b_0+b_1+h_0}\right)h_0^2 + \left(\frac{2b_1+h_0}{b_0+b_1+h_0}\right)b_0 h_0^2\right]}, \tag{5}$$

b_0 and b_1 are slip lengths at the lower and upper surface facing each other. Equations (3), (4), and (5) are derived for rigid motion of the plate by solving Reynolds

This manuscript was accepted by J. Appl. Phys. Click here to see the version of record.

equation with ambient pressure boundary conditions on all the four sides of a rectangular domain[17]. **This model is obtained for incompressible flow, and hence, it is valid for low operating frequencies. It captures the rarefaction effect through the slip lengths at the boundaries.**

- To consider the effect of flexural motion of a fixed-fixed beam vibrating near a fixed plate, the squeeze film damping model under ambient pressure condition is obtained by solving the Reynolds equation with zero-pressure condition at free boundaries and a no-flow condition at the fixed-boundaries. The Reynolds equation is solved with the assumptions[27] under which the flow is assumed to be (a) two dimensional due to the pressure gradient along the two planar directions, and (b) isothermal and viscous with weak compressibility provided through $\rho \propto P$, where, P is the pressure. This model is accurate for $h_0/b < 0.1$. For $h_0/b > 0.1$, the 3D flow effect can be approximately modeled by writing an effective dimension $b_{\text{eff}} = b + \xi h_0$, where, ξ is a correction factor associated with b_{eff}. The quality factor from the squeeze film losses of a fixed-fixed beam can be computed from the expression obtained by Zhang *et al.*[27], $Q_{\text{s2}} = \frac{\sqrt{1-m_{\text{sqa}}}}{c_{\text{sqa}}}$ where, m_{sqa} and c_{sqa} are the squeeze inertia number and the squeeze damping number respectively. We write the exact mode shape of the fixed-fixed beam as[20,27], $\chi(x) = \cosh(\alpha x/a) - \cos(\alpha x/a) + \gamma[\sinh(\alpha x/a) - \sin(\alpha x/a)]$, where $\gamma = -\frac{[\cosh(\alpha)-\cos(\alpha)]}{[\sinh(\alpha)-\sin(\alpha)]}$, x/a is a non-dimensional geometric factor, a is the beam length and α is the frequency parameter. The parameter α is obtained by solving the frequency equation, $\cos(\alpha)\cosh(\alpha) - 1 = 0$ (for the fundamental mode, $\alpha = 4.73$)[20]. The expressions for squeeze inertia and the squeeze damping numbers are written as,

$$m_{\text{sqa}} = \frac{\mu^2 a^4}{\pi^2 P_a \rho_s d_0 h_0^5}\left[\sum_{m=\text{even}}^{\infty}\sum_{n=\text{odd}}^{\infty}\frac{2304 a_m^2}{n^2}\frac{1}{[(m^2\pi^2+n^2\pi^2\beta^2)^2+\sigma^2]} + \sum_{n=\text{odd}}^{\infty}\frac{1152 a_0^2}{n^2(n^4\pi^4\beta^4+\sigma^2)}\right],$$

$$c_{\text{sqa}} = \frac{\mu a^4}{\sqrt{3\rho_s E}\alpha^2 d_0^2 h_0^3}\left[\sum_{m=\text{even}}^{\infty}\sum_{n=\text{odd}}^{\infty}\frac{1152 a_m^2}{n^2\pi^2}\frac{(m^2\pi^2+n^2\pi^2\beta^2)}{[(m^2\pi^2+n^2\pi^2\beta^2)^2+\sigma^2]} + \sum_{n=\text{odd}}^{\infty}\frac{576 a_0^2\beta^2}{(n^4\pi^4\beta^4+\sigma^2)}\right].$$

where, a_p is given by $a_p = \frac{\alpha\sinh(\alpha)}{\alpha^2+p^2\pi^2} + \gamma\frac{\alpha\cosh(\alpha)-\alpha}{\alpha^2+p^2\pi^2} - \frac{\sin(p\pi-\alpha)}{2(p\pi-\alpha)} - \frac{\sin(p\pi+\alpha)}{2(p\pi+\alpha)} - \gamma\frac{1-\cos(\alpha-p\pi)}{2(\alpha-p\pi)} - \gamma\frac{1-\cos(\alpha+p\pi)}{2(\alpha+p\pi)}$, $p = 0$ and $1, 3, 5, ..., m$. A ready evaluation of the squeeze film quality factor (Q_{s2}), valid for the squeeze number, $\sigma = \frac{12\mu_{\text{eff}}\omega a^2}{P_a h_0^2} \ll 1000$ and aspect ratio, $\beta = a/b > 10$ is obtained by using the expression for the squeeze inertia and damping numbers written as[27], $m_{\text{sqa}} = 1.1977\frac{\mu_{\text{eff}}^2 b_{\text{eff}}^4}{P_a\rho_s d_0 h_0^5}$, $c_{\text{sqa}} = 0.1525\frac{\mu_{\text{eff}} a_{\text{eff}}^2 b_{\text{eff}}^2}{\sqrt{\rho_s E} h_0^3 d_0^2}$. For the fundamental mode of the resonator, the constants $\alpha = 4.73$, $a_0 = 0.831$. The constant a_0 is obtained by setting p to zero in the expression for a_p (with γ = -0.983). For the air gap thickness set to the experimental values of 750 nm, 660 nm, 460 nm and 250 nm, respectively, the corresponding computed squeeze number, σ, is 32, 39, 66, and 132. To capture the rarefaction effect, we invoke the effective viscosity model[23,24], and use $\mu_{\text{eff}} = \frac{\mu}{Q_{\text{rt}}}$, where Q_{rt} is the non-dimensional relative flow rate given by, $Q_{\text{rt}} = 1 + 3 \times 0.01807 \times \sqrt{\pi}/D + 6 \times 1.35355 \times D^{-1.17468}$, with $D = \frac{\sqrt{\pi}}{2\text{Kn}}$. For the range of air gaps (250 nm–750 nm) considered in the present study, the fluid flow regime varies from the transition flow to slip flow. Here, μ_{eff} is obtained for gaseous slip flow under ambient pressure and temperature conditions. However, the variation in pressure and temperature of the surrounding air can be captured while computing the mean free path or velocity slip[24,28,29]. The current formulation of the slip velocity is for gaseous flow[24], however, an appropriate slip model can be selected for other fluids such as liquids or moisture[30].

C. Comparison with experimental results

In this section, we compare the results from different models with experimental results taken from Verbridge et al[12]. In all the cases, we take effective length of the beam as $a = 12.5\mu$m. **Figures 2(a) and (b) illustrate that all drag models fail to match experimental results for sufficiently large b. For small b, the match between model and experimental data appears best for models Q_{d1} and Q_{d4} (in Fig.2(b)). While the models Q_{d1}, Q_{d2}, and Q_{d3} are independent of air-gap thickness, Q_{d4} is a function of h_0. Moreover, the model Q_{d1} captures drag based on the thin disc model, and models Q_{d2} and Q_{d3} capture the drag based on the "sphere" model without and with inertial effects. Therefore, to fit the damping due to drag force in the range of smaller values of beam width, we choose a specific thin disc**

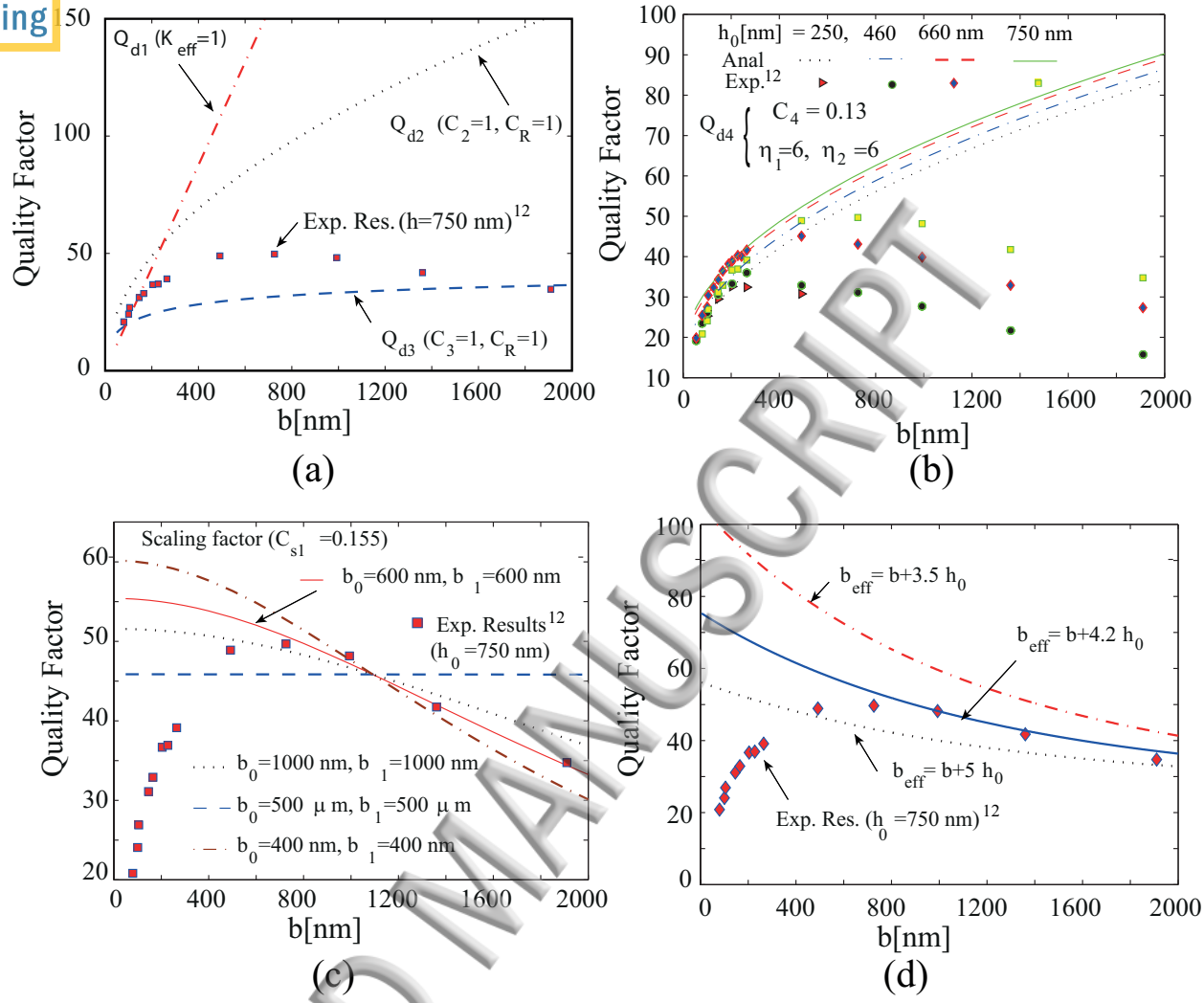

FIG. 2. Comparison for drag force based quality factor computed from (a) Q_{d1} ($K_s = 1$), Q_{d2} ($C_2 = 1$ and $C_R = 1$), and Q_{d3} ($C_3 = 1$ and $C_R = 1$) with experimental results for $h_0 = 750$ nm, and (b) Q_{d4} with experiments for $h_0 = 250,\ 460,\ 660$, and 750 nm, respectively. Comparison of squeeze-film based quality factors using (c) Q_{s1} ($C_{s1} = 0.155$) at different slip lengths b_0 and b_1, and (d) Q_{s2} at different effective lengths with experimental results for $h_0 = 750$ nm.

model Q_{d1}, and a generalized "sphere" model Q_{d3} for further analysis.

Similarly, Figures 2(c) and (d) show the comparison of squeeze film models Q_{s1} and Q_{s2} with experiments. Figures show that both the models fail to match with experiments for sufficiently small width. However, both require fitting parameters to match the experimental results for larger width. While Q_{s1} requires two fitting parameters, namely, slip length and scaling constant, Q_{s2} requires

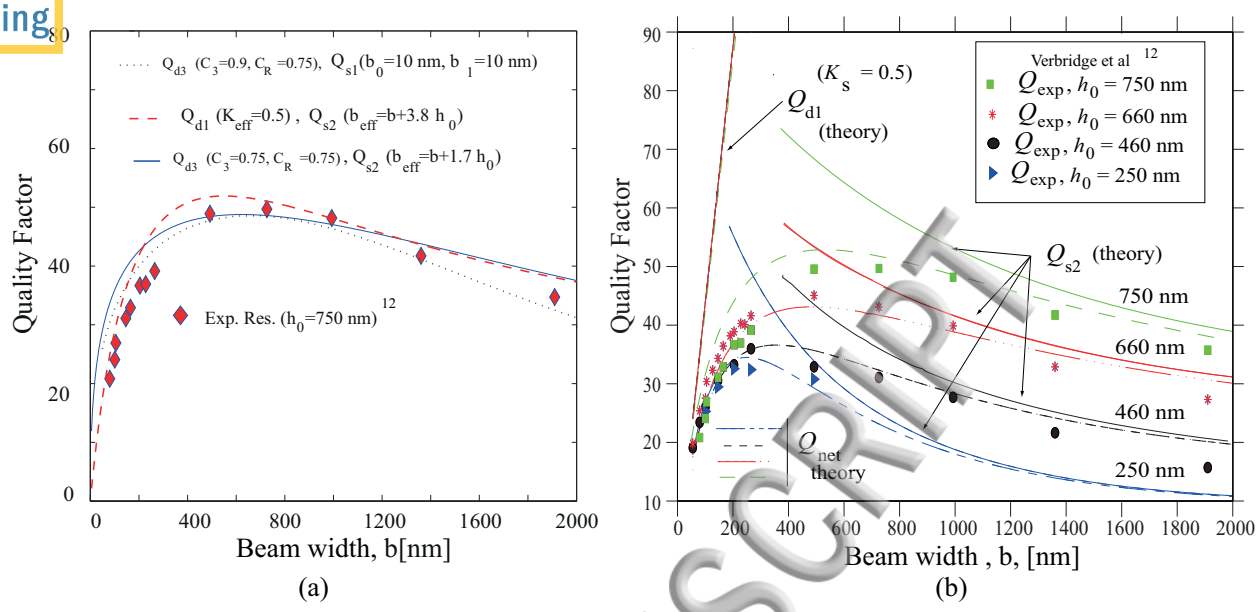

FIG. 3. (a) Comparison of combined quality factor due to drag and squeeze film using $Q_{d3}(C_3 = 0.9$ and $C_R = 0.75)$ and $Q_{s2}(b_0 = 10\text{nm}$ and $b_1 = 10\text{nm})$, $Q_{d1}(K_{\text{eff}} = 0.5)$ and Q_{s2} $(b_{\text{eff}} = b + 3.8h_0)$, $Q_{d3}(C_3 = 0.9$ and $C_R = 0.75)$ and Q_{s2} $(b_{\text{eff}} = b + 1.7h_0)$ with experiments for $h_0 = 750\text{nm}$; (b) Comparison of theoretically computed analytical results using $Q_{d1}(K_{\text{eff}} = 0.5)$ and Q_{s2} $(b_{\text{eff}} = b + \xi h_0$, where $\xi = 3.2,\ 3.8,\ 4.1,\ 3.8$ for $h_0 = 250\text{nm}$, 460nm, 660nm and 750nm, respectively) with experimental results at different air-gap thickness.

only one fitting parameter, *i.e.*, effective width. Moreover, Q_{s1} is valid for an incompressible fluid only, while the validity of Q_{s2} can be extended to fluid with low compressibility.

To compare the combined effect of drag and squeeze film damping, we take different combinations of drag models, Q_{d1} and Q_{d3}, and squeeze film models, Q_{s1} and Q_{s2} and compute the net quality factor using eqn. (1). Figure 3(a) shows the comparison of Q_{net} computed with combinations $Q_{d3}(C_3 = 0.9$ and $C_R = 0.75)$ and $Q_{s1}(b_0 = 10\text{nm}$ and $b_1 = 10\text{nm})$, $Q_{d1}(K_{\text{eff}} = 0.5)$, and Q_{s2} $(b_{\text{eff}} = b + 3.8h_0)$, $Q_{d3}(C_3 = 0.9$ and $C_R = 0.75)$ and Q_{s2} $(b_{\text{eff}} = b + 1.7h_0)$ with experimental results for $h_0 = 750\text{nm}$. Although all the combinations with different fitting parameters approximate the measured results nearly equally well, we use the combination based on Q_{d1} and Q_{s2} for further analysis, **as Q_{s2} is more general than Q_{s1}.** Using Q_{d1} with $K_{\text{eff}} = 0.5$ and Q_{s2} with $b_{\text{eff}} = b + \xi h_0$, we find the fitting parameter $\xi = 3.2,\ 3.8,\ 4.1$ and 3.8 corresponding to h_0 =250 nm, 460 nm, 660 nm and

750 nm for the closest fits with experimental results as shown in Fig. 3(b). The fits to the squeeze film quality factor, Q_{s2} exhibit a monotonic increase in the squeeze film losses with increase in the beam widths. The pressure applied by the fluid on to the plate rises with an increase in the beam width, resulting in a decrease in Q_{s2} for a fixed air gap thickness. As the air-gap thickness decreases, Q_{s2} exhibits a steeper descent with $Q_{s2} \propto (1/b)^2$ for a given air-gap thickness over a large range of beam widths (from 55 nm to 300 nm). The theoretical fits match well with experimental results. The net computed quality factor, Q_{net}, has a dominant contribution from squeeze film losses at higher beam widths, while the drag force damping computed using Q_{d1} dominates in slender beams.

Finally, the net computed quality factor can be found from $Q_{\text{net}}^{-1} = Q_{\text{s2}}^{-1} + Q_{\text{d1}}^{-1}$, which is dominated by viscous losses. The calculated Q_{net}^{-1} corroborates the experimental results, and is found to have a maximum at a characteristic beam width, at which neither of the viscous dissipation mechanisms dominates, resulting in an optimized high-Q resonator geometry for a chosen air gap thickness. It is seen from Fig. 3(b) that the maximum value of Q_{net} shifts to higher beam width with larger air gap thickness. We find that the drag force mechanism (Q_{d1}) provides larger energy loss for smaller values of b/h_0 ratio, and the squeeze film losses dominates for larger values of b/h_0 ratio. In the range, $0.45 < b/h_0 < 1$ (the crossover regime shown in Fig. 3(b)), both mechanisms provide comparable damping. To further quantify the relative dominance of squeeze film damping over drag dissipation in the next section, we take $b_{\text{eff}} = b + 3.5h_0$.

III. FINITE SIZE EFFECTS FROM THE DOUBLY CLAMPED BEAM

In this section, we extend the present model to predict the variation of Q_{net} with b if the air gap thickness as well as length were varied beyond the values explored in the study by Verbridge *et al.*[12]. We have used Q_{d1} with fitting coefficient $K_{\text{eff}} = 0.5$ and Q_{s2} with $b_{\text{eff}} = b + 3.5h_0$ to compute Q_{net} to analyze the influence of air-gap thickness h_0 and beam length a on Q_{max} and b_{max}, respectively, as follows:

- *Effect of air-gap thickness:* Figure 4(a) shows the variation of Q_{net} with beam width, b, in which Q_{max} is found to saturate at higher h_0 and remains constant with b. For larger airgaps, b_{max} does not attain a maximum but increases slowly with beam width. Thus squeeze film losses (dominant for large widths) decrease as the height h_0 increases[27].

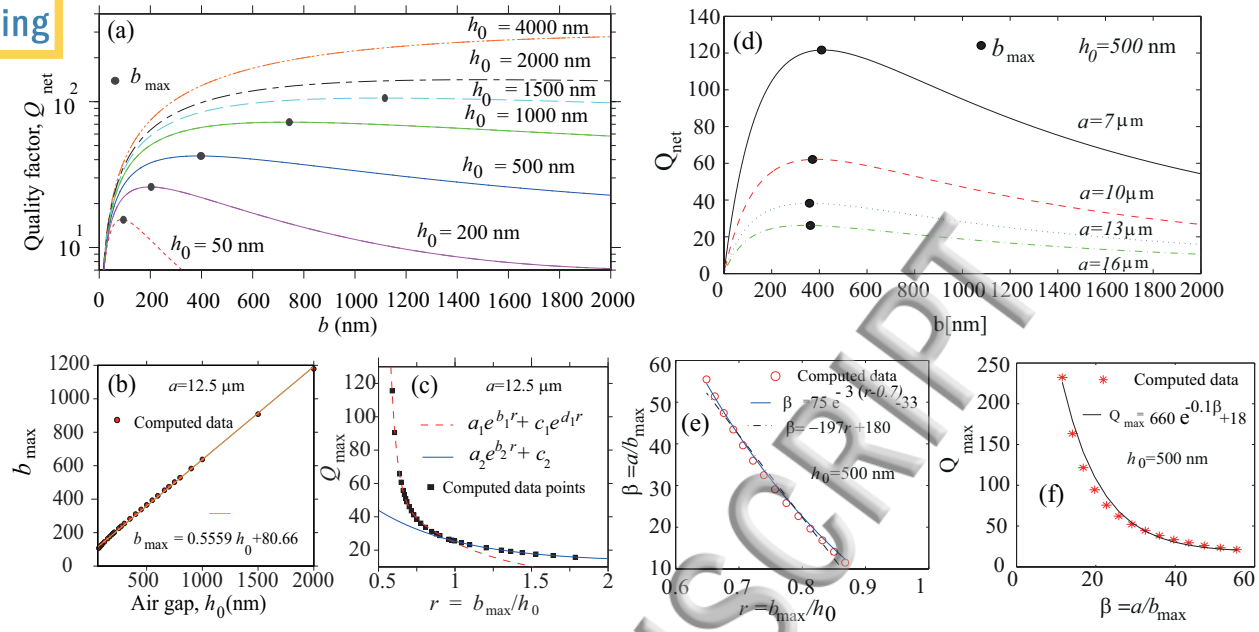

FIG. 4. (a) Variation in the net quality factor computed from $Q_{d1}(K_{\text{eff}} = 0.5)$ and Q_{s2} ($b_{\text{eff}} = b + 3.5h_0$ with beam width, b, for various air gap thicknesses. The black dots mark the optimum beam width $b_{\max}$ to achieve $Q_{\max}$ for a given air-gap thickness, h_0; (b) $b_{\max}$ varies with air-gap thickness, h_0 as $b_{\max} = 0.5559h_0 + 80.66$; (c) The maximum quality factor, $Q_{\max}$, varies exponentially with the aspect ratio $b_{\max}/h_0$; (the coefficients corresponding to curve fit for 0.5 $< r <$ 0.95, are $a_1 = 1.288 \times 10^8$, b_1 = -24.62, c_1 = 141.5, d_1 = -1.755, and the corresponding coefficients for the aspect ratio, r in the range $0.95 < r < 2$, are a_2 = 77.24, b_2 = -1.823, and c_2 = 12.87, respectively. The parameters for simulation are: $a_{\text{eff}} = 12.5$ μm, $b_{\text{eff}} = b + 3.5h_0$ μm, d_0 = 140 nm, and K_s =0.5). (d) Variation of $Q_{\max}$ with beam width b for different lengths a, and the corresponding variation of (e) $\beta = a/b_{\max}$ with $r = b_{\max}/h_0$ and (f) $Q_{\max}$ and $\beta = a/b_{\max}$.

Using the expressions for m_{sqa} and c_{sqa}, the expression for the net quality factor can be used to find the maximum value of the quality factor ($Q_{\max}$) and the corresponding value of the optimum beam width ($b_{\max}$). For a range of air gap thicknesses h_0, the corresponding width $b_{\max}$ can be obtained from $b_{\max} = 0.5559h_0 + 80.66$ or $\frac{b_{\max}}{a} = 0.5559\frac{h_0}{a} + 0.00645$ for 50 nm $< h_0 <$ 1.5 μm as shown in Fig. 4(b). The relation between $Q_{\max}$ and $r = b_{\max}/h_0$ are shown in Fig. 4(c) and are found as $a_1e^{b_1r} + c_1e^{d_1r}$ for $0.5 < r <$ 0.95 and $a_2e^{b_2r} + c_2$ for $0.95 < r < 2$. Here, $a_1 = 1.288 \times 10^8$, b_1 = -24.62, c_1 = 141.5, d_1 = -1.755, a_2 = 77.24, b_2 = -1.823, and c_2 = 12.87. It is noticed that two sources of dissipation influence the damping behavior corresponding to $Q_{\max}$

This manuscript was accepted by J. Appl. Phys. Click here to see the version of record.

in the range of $0.5 < r < 0.95$, whereas, only squeeze film dominates the damping behavior in the range of $0.95 < r < 2$.

- *Effect of beam length:* Similarly, Figure 4(d) shows the variation of Q_{net} with b for different beam lengths when the air-gap thickness is maintained at $h_0 = 500$ nm and variation in frequency is considered using Eqn. (2). As the beam length increases, $b_{\max}$ tends to a constant value, while $Q_{\max}$ decreases asymptotically to 20 for a given air-gap thickness $h_0 = 500$ nm. Fig. 4(e) shows the variation of $\beta = a/b_{\max}$ **and** $r = b_{\max}/h_0$. For large beam length, optimum value of $r = b_{\max}/h_0$ can be taken in the range of 0.6 to 0.7. The linear and exponential approximations of $\beta = a/b_{\max}$ and $r = b_{\max}/h_0$ can also be found as $\beta = -197r + 180$ and $\beta = 75e^{-3(r-0.7)} - 33$, respectively. Figure 4(f) also shows that $Q_{\max}$ decreases exponentially with $\beta = a/b_{\max}$ as $Q_{\max} = 600e^{-0.1\beta} + 18$. As the beam length increases beyond a certain value, most of the damping is due to 1-D flow and is entirely dependent on the beam width to gap ratio. Under these conditions, 1-D models can be used to compute damping forces.

The empirical fits, which serve as a recipe to achieve a high-Q structure for various ranges of the aspect ratios (β and r) will prove to be useful in designing high performance devices. Finally, we state that the present study can be of significance in understanding the fluid damping in a multidisciplinary area. Although the present formulation is suited for gaseous flow, the fluid damping in liquid can be obtained by suitably modifying the slip condition at the boundary[30].

IV. CONCLUSIONS

Our central interest in the present study was to identify the dominant viscous losses and quantify the associated quality factors for a range of beam widths. Our findings match well with the experimental results. The present model provides insight into finite size effects and yields an optimized doubly clamped geometry to achieve a high-Q beam resonator. We have identified a range for the aspect ratio (b/h_0), at which the two viscous losses compete with each other. We have also found the limiting cases of aspect ratios for a fixed length of the beam at which only the squeeze film damping or the drag force damping alone contributes to the net quality factor. The present model is applicable as long as the doubly clamped

beam geometry is so choosen to be within the limits of the thin beam theory. For thick beams, the search for optimum-Q requires a separate detailed study.

ACKNOWLEDGMENTS

This work was partially supported by Grant no. NSF ECCS 1001742, DMR 1120296, MIT084 of DeitY, Government of India, and CSIR 22(0696)/15/EMR-II.

REFERENCES

[1]D. R. Southworth, L. M. Bellan, Y. Linzon, H. G. Craighead, and J. M. Parpia, Appl. Phys. Lett. **96**, 163503 (2010).

[2]A. K. Pandey, K.P. Venkatesh and R. Pratap, Sadhana, 34(4), 651-662 (2009).

[3]D. J. Joe, Y. Linzon, V. P. Adiga, R. A. Barton, M. Kim, B. Ilic, S. Krylov, J. M. Parpia, and H. G. Craighead, J. Appl. Phys. **111**, 104517 (2012).

[4]B. Ilic, H. G. Craighead, S. Krylov, W. Senaratne, C. Ober, and P. Neuzil, J. Appl. Phys. **95**, 3694 (2004).

[5]Y. Yang, C. Callegari, X. Feng, K. Ekinci, and M. Roukes, Nano Lett. **6**, 583 (2006).

[6]A. K. Pandey, PhD Thesis, IISc Bangalore, (2007).

[7]R. Lifshitz and M. L. Roukes, Phys. Rev. B **61**, 5600 (2000).

[8]J. A. Judge, D. M. Photiadis, J. F. Vignola, B. H. Houston and J. Jarzynski, J. Appl. Phys. **101**, 013521 (2007).

[9]S. D. Vishwakarma, A. K. Pandey, J. M. Parpia, D. R. Southworth, H. G. Craighead and R. Pratap, J. Microelctromech. Syst. **23**, 334 (2014).

[10]T. Ikehara, J. Lu, M. Konno, R. Maeda, and T. Mihara, J. Micromech. Microeng. **17**, 2491 (2007).

[11]X. Xia, and X. Li, Rev. Sci. Instrum. **79**, 074301 (2008).

[12]S. S. Verbridge, R. Ilic, H. G. Craighead, and J. M. Parpia, Appl. Phys. Lett. **93**, 013101 (2008).

[13]E. C. Bullard, J. Li, C. R. Lilley, P. Mulvaney, M. L. Roukes, and J. E. Sader, Phys. Rev. Lett. **112**, 015501 (2014).

[14]J. E. Sader, J. Appl. Phys. **84**, 64 (1998).

[15]S. Ramanathan, D. L. Koch, and R. B.Biladvala, Phys. Fluids **22**, 103101 (2010).

[16]C.Lissandrello, V. Yakhot, and K. L. Ekinci, Phys. Rev. Lett. **108**, 084501 (2012).

[17]A. Drezet, A. Siria, S. Huant and J. Chevrier, Phys. Rev. E **81**, 046315 (2010).

[18]C. D. F. Honig, J. E. Sader, P. Mulvaney, and William A. Ducker, Phys. Rev. E **81**, 056305 (2010).

[19]A. P. Bowles and W. A. Ducker, Phys. Rev. E **83**, 056328 (2011).

[20]S. S. Rao, *Vibration of Continuous Systems* (John Wiley & Sons, Inc., New Jersey, 2007).

[21]J. Happel and H. Brenner, *Low Reynolds Number Hydrodynamics with Special Applications to Particulate Media*, (Prentice-Hall Inc., Englewood Cliffs, New Jersey, 1965).

[22]S. Kim and S. J. Karrila, *Microhydrodynamics*, (Butterworth-Heinemann, Boston, 1991).

[23]A. K. Pandey and R. Pratap, J. Micromech. Microeng. **18**, 105003 (2008).

[24]Li W.-L., Nanotechnology **10**, 440 (1999).

[25]R. B. Bhiladvala and Z. J. Wang, Phys. Rev. E **69**, 036307 (2004).

[26]M. H. Bao and H. Yang, Sens. Actuators, A **136**, 3 (2007).

[27]C. Zhang, G. Xu, and Q. Jiang, J. Micromech. Microeng. **14**, 1302 (2004).

[28]A. K. Pandey and R. Pratap, J. Micromech. Microeng. **17**, 2475-2484 (2007).

[29]C. E. Siewert, Phys. Fluids **15(6)**, 1696-1701 (2003).

[30]J. B. Shukla, S. Kumar and P. Chandra, Wear, **60**, 253 268 (1980).

(a)

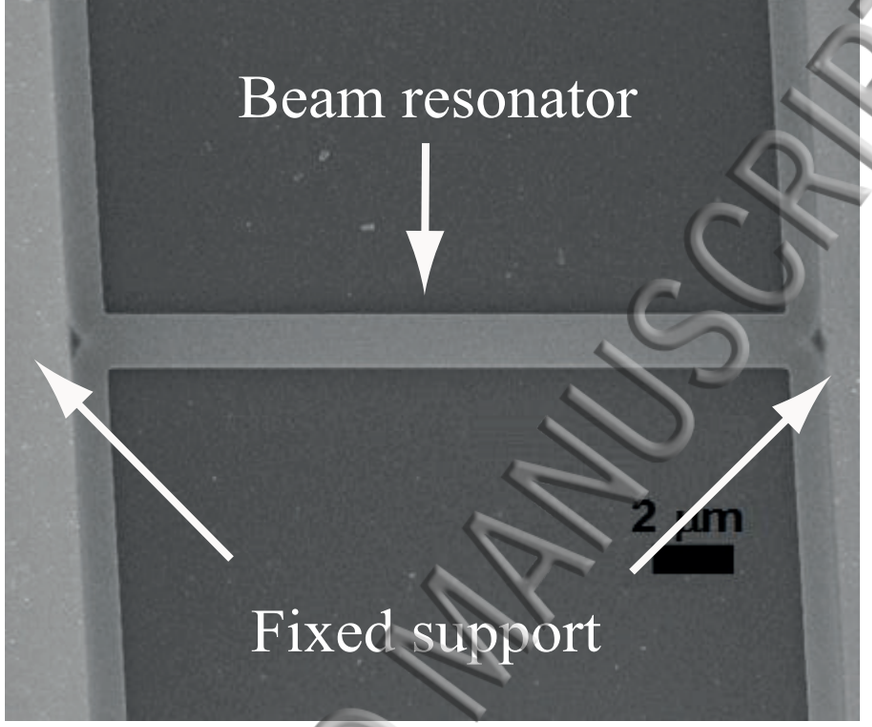

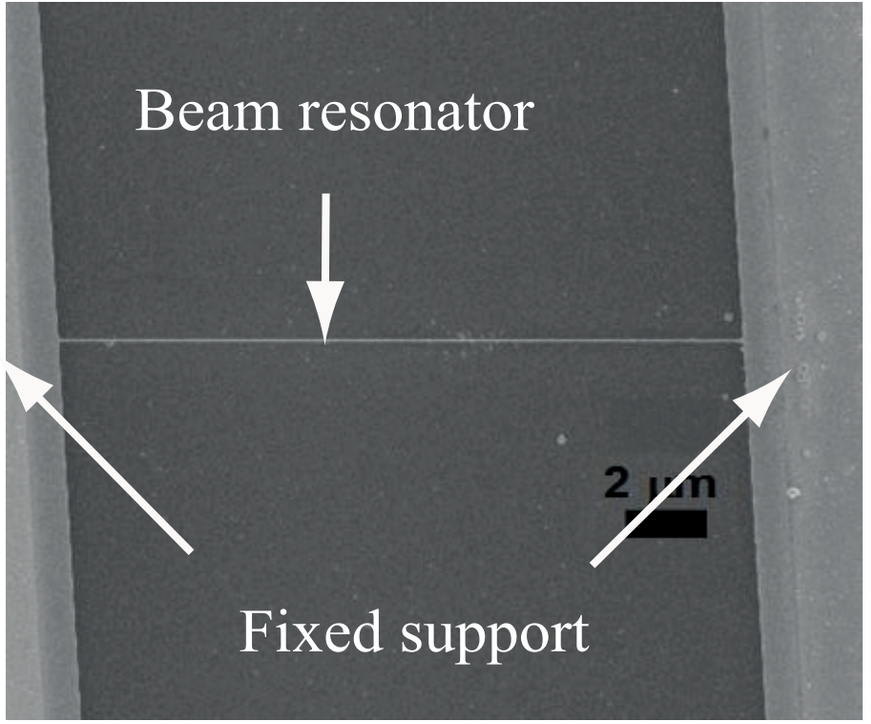

(b)

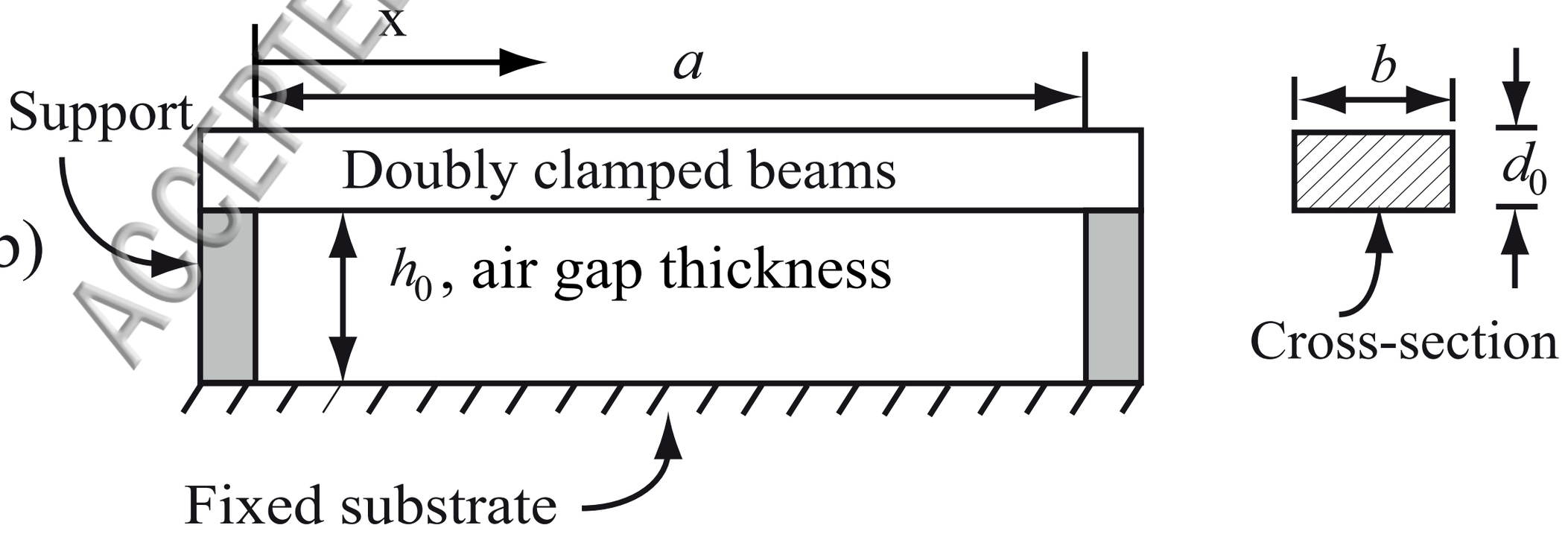

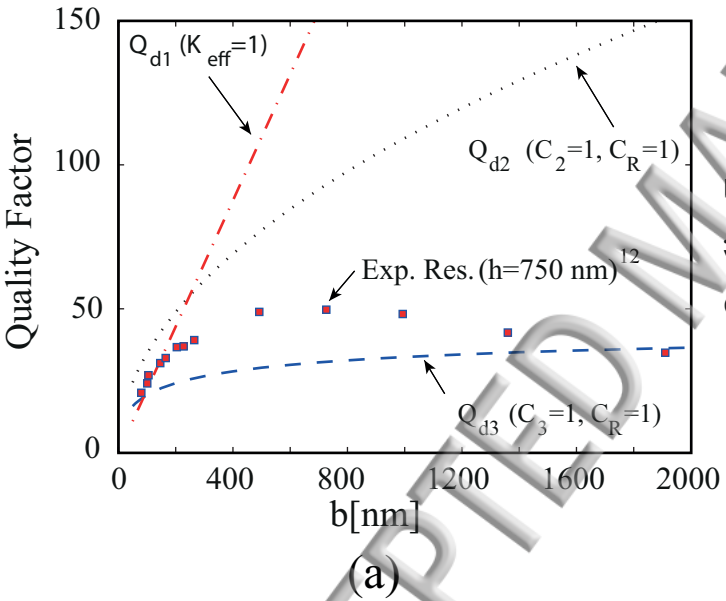

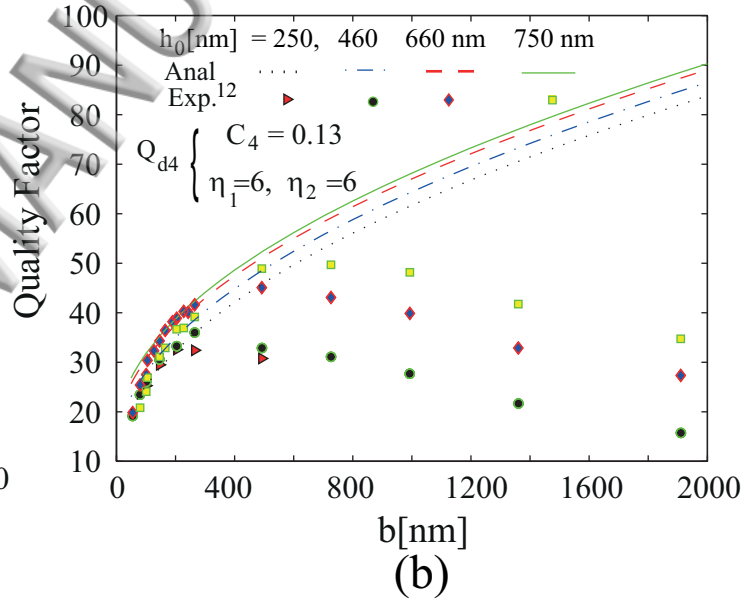

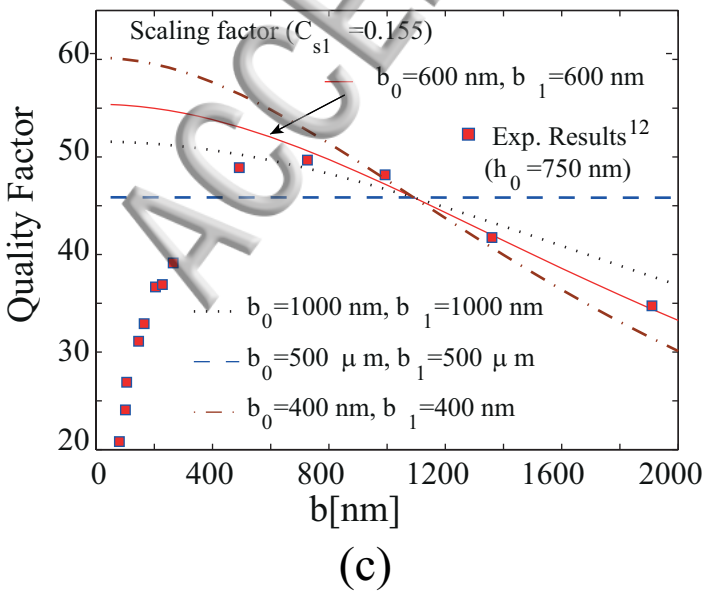

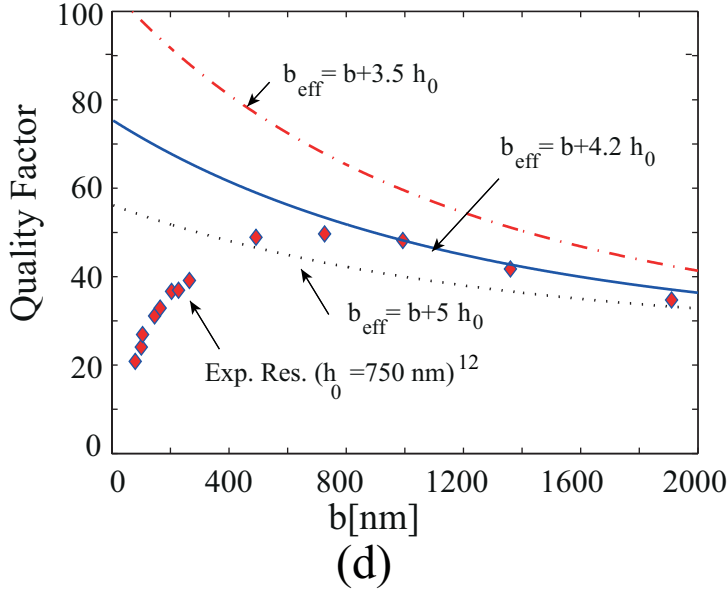

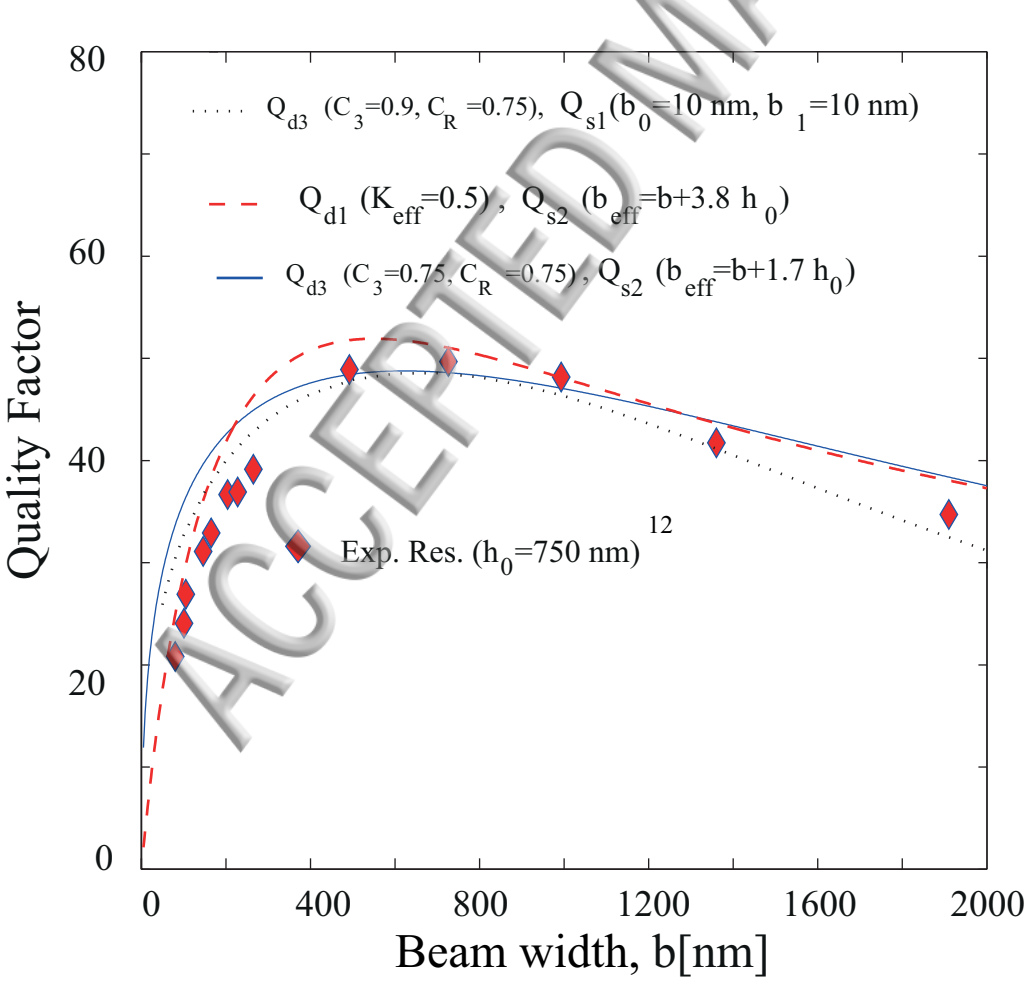

(a)

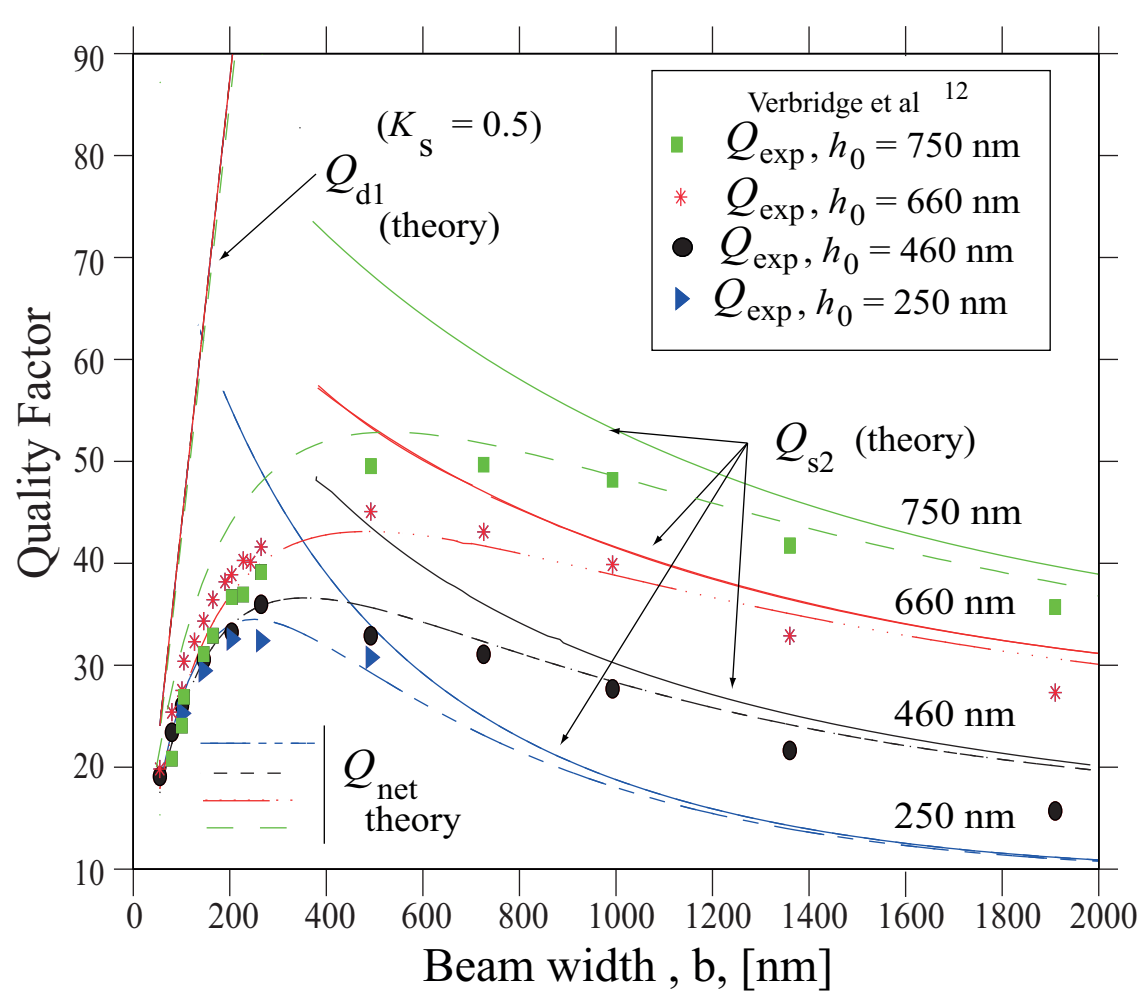

(b)